Dalton Transactions

ROYAL SOCIETY OF CHEMISTRY

PAPER

View Article Online
View Journal | View Issue

Cite this: *Dalton Trans.*, 2022, **51**, 5596

Manipulating the spin crossover behaviour in a series of cyanide-bridged $\{Fe^{III}_2Fe^{II}_2\}$ molecular squares through NCE^- co-ligands†

Maolin You,[a,b] Giang T. Nguyen, [b] Dong Shao, [a] Te Wang,[a] Xiao-Yong Chang,[a] Liviu Ungur *[b] and Yuan-Zhu Zhang *[a]

Received 7th January 2022,
Accepted 4th March 2022

DOI: 10.1039/d2dt00058j

rsc.li/dalton

Manipulating the transition temperature ($T_{1/2}$) of spin-crossover (SCO) complexes capable of fulfilling practical criteria through different synthetic strategies is one of the main focuses in the field of molecular magnetism. The reaction of the tricyanometallate precursor $[(Tp^*)Fe^{III}(CN)_3]^-$ and Fe(II) salt with the "facially" tridentate ligand tris(2-pyridyl)phosphine oxide (TPPO) and NCE^- anions afforded three isostructural $\{Fe^{III}_2Fe^{II}_2\}$ square complexes $\{[(Tp^*)Fe^{III}(CN)_3]_2[Fe^{II}(TPPO)]_2[NCE]_2\}\cdot Sol$ (E = S, Sol = $2CH_3OH\cdot 6H_2O$, **1**; E = Se, Sol = $2MeCN\cdot 2CH_2Cl_2\cdot 2H_2O$, **2**; E = BH_3, Sol = $4CH_3OH\cdot 2MeCN$, **3**). Detailed structural analysis, variable-temperature IR analysis, magnetic susceptibility measurements and DFT calculations revealed that all compounds exhibit complete and one-step SCO behaviour between the $\{Fe^{III,LS}_2Fe^{II,HS}_2\}$ and $\{Fe^{III,LS}_2Fe^{II,LS}_2\}$ electronic states. As the ligand field increases from NCS^- to $NCSe^-$ to $NCBH_3^-$, $T_{1/2}$ shifts dramatically from 214 to 250 to 288 K for **1**, **2** and **3**, respectively, demonstrating another effective way to tune the SCO properties of the $[Fe^{III}–CN–Fe^{II}]$ systems through the introduction of NCE^- co-ligands.

Introduction

Spin crossover (SCO) solids in discrete and polymeric transition complexes are promising candidates to engineer and fabricate molecule-based switches and electronic devices.[1–4] Reversible switching between the enthalpy-favoured low-spin (LS) and entropy-favoured high-spin (HS) states can be triggered by various external stimuli (light irradiation, temperature, pressure, *etc.*), associated with drastic changes in structural, magnetic, and optical behaviours.[5] Particularly, some of these materials may show photo-induced spin transition behaviour, named light-induced excited spin state trapping (LIESST) or ligand-driven light-induced spin change (LDLISC), providing a promising way to modulate various physical properties at the molecular level.[6] Towards practical applications, SCO complexes with the pronounced hysteresis region centred at room temperature (RT) are highly desired.[7] Although intensive endeavours have been devoted to producing various SCO materials, controlling the SCO properties at will within the defined complex mode is still challenging for chemists.

Polymorphism studies on SCO complexes have provided an extraordinary view to reveal the impact of crystal packing on the spin transition (ST).[8] For example, Hagiwara and coworkers reported a polymorphism-dependent transition temperature ($T_{1/2}$) shift of 100 K that spans RT due to the differences in the weak intermolecular CH···X hydrogen bonds.[9] Through judicious ligand modification, the synthesis of complexes with similar structures is another well-established strategy for synthetic chemists to explore the structure–property relationships systematically. For example, the partially capped tricyanoiron(III) anions of $[(Tp^R)Fe(CN)_3]^-$ (Tp^R = poly(pyrazol-1-yl)borate)[10] have been widely used for constructing structurally-related SCO-active complexes, including $\{Fe^{III}_{24}Fe^{II}_{18}\}$ clusters,[11] $\{Fe^{III}_2Fe^{II}\}$ trinuclear complexes,[12] $\{Fe^{III}_2Fe^{II}_2\}$ squares,[13] $\{Fe^{III}_4Fe^{II}_4\}$ cubes,[14] $\{Fe^{III}_2Fe^{II}\}_n$ one-dimensional (1D) chains[15] or two-dimensional (2D) chains.[16] Recently, our group demonstrated in a series of $\{Fe^{III}_2Fe^{II}\}$ complexes that the SCO behaviour (transition speed (abrupt/gradual), the transition temperature ($T_{1/2}$), and thermal hysteresis, *etc.*) may be finely tuned by engineering the electric and steric effects as well as intermolecular interactions *via* equipment of different substituent groups on a given ligand.[17] Moreover, we successfully prepared two $\{Fe^{III}_4Fe^{II}_4\}$ cubes that exhibited rare and reversible metal-to-

[a]*Department of Chemistry, Southern University of Science and Technology, Shenzhen, 518055, P. R. China. E-mail: zhangyz@sustech.edu.cn*

[b]*Department of Chemistry, National University of Singapore, 3 Science Drive 3, Singapore 117543*

†Electronic supplementary information (ESI) available: Tables of selected bonds and angles, and TGA analysis, and magnetic data, and PXRD spectra, and DFT calculation results. CCDC 2125760–2125765. For ESI and crystallographic data in CIF or other electronic format see DOI: 10.1039/d2dt00058j

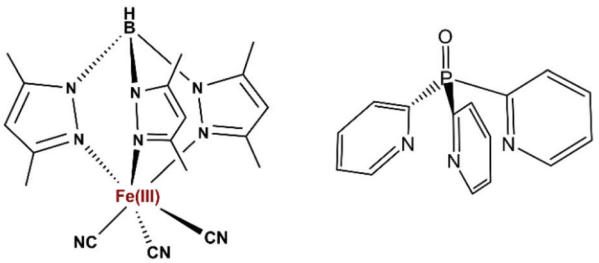

Scheme 1 The structures of the $[(Tp^*)Fe(CN)_3]^-$ building block (left) and the tridentate TPPO ligand (right).

metal charge transfer (MMCT) behaviour rather than the more prevalent SCO behaviour in the $[Fe^{III}–CN–Fe^{II}]$ system.[18] However, whether it would display MMCT or SCO behaviour for a given mixed-valence homometallic compound is still unclear, and more concerns are thus needed for better understanding this encrypted system.

It has been known that the SCO process of the mononuclear complexes of $[(L)Fe^{II}(NCE)_2]$ may be engineered in a predictable way *via* the substitution of NCE^- (E = S, Se, BH_3) co-ligands.[19] Generally, $T_{1/2}$ increases with the increase of ligand strength ($NCS^- < NCSe^- < NCBH_3^-$). However, this strategy has not been adopted in the homometallic cyanometallate (Fe–Fe) system featuring electronic versatility, which may exhibit SCO and/or MMCT behaviours.[18,20] Herein, we report the syntheses, crystal structures, DFT calculations, and magneto-structural study of three isostructural $\{Fe^{III}_2Fe^{II}_2\}$ molecular squares, in which the cyanide-bridged Fe^{III} and Fe^{II} centres alternately reside in the corners and each Fe^{II} centre is further coordinated to a capping tridentate ligand (TTPO, Scheme 1) as well as one NCE^- co-ligand, giving the neutral $\{[(Tp^*)Fe(CN)_3]_2[Fe(TPPO)]_2[NCE]_2\}$ square cores. All three compounds display complete and one-step SCO behaviour with $T_{1/2}$ shifting from 214 K (**1**) to 250 K (**2**) to 288 K (**3**) due to the increasing ligand strength ($NCS^- < NCSe^- < NCBH_3^-$).

Results and discussion

Treatment of $Fe^{II}(OTf)_2$, $[(PPh_3Me)][(Tp^*)Fe^{III}(CN)_3]$, TPPO, and NCE^- co-ligands in mixed solvents of methanol and acetonitrile with a 1 : 1 : 1 : 1 ratio afforded red block crystals of complexes **1**, **2**, and **3**, respectively. The purity of **1**–**3** in bulk was confirmed by elemental analysis (EA) and power X-ray diffraction (PXRD) measurements (Fig. S1–S3†). The thermogravimetric analysis (TGA, Fig. S4†) of **1**, **2**, and **3** displayed a one-step weight loss for the lattice solvents at around 80 °C, and then a platform up to 220 °C, suggesting the considerable thermal stability of the desolvated phase. Single crystal X-ray diffraction (SC-XRD) data were collected for **1**, **2**, and **3**, respectively, at both 100 and 300 K. The results revealed that all complexes are isostructural and crystallize in the orthorhombic space group *Fdd*2 at both temperatures (Table 1). The asymmetric unit of **1**, **2**, and **3** contains half a square with crystallographically unique Fe^{III} and Fe^{II} (Fig. S5–S7†) ions. Adjacent $[(Tp^*)Fe^{III}(CN)_3]^-$ and $[(TPPO)Fe^{II}]$ units (in a 2 : 2 ratio) reside in alternate corners of a molecular square and are bridged by cyanide group. Each Fe^{II} ion bears one additional terminal NCE^- co-ligand which adopts an *anti*-orientation relative to the $\{Fe^{III}_2(\mu\text{-}CN)_4Fe^{II}_2\}$ square plane (Fig. 1), affording an $[Fe^{II}N_6]$ coordination environment. For compound **1** at 100 K, the Fe2–N bond lengths are in the range of 1.942(2)–2.018(2) Å, whereas the Fe1–C and Fe1–N bond lengths are in the ranges of 1.922(3)–1.947(3) Å and 1.985(2)–2.009(2) Å, respectively, indicating the LS Fe^{III} and LS Fe^{II} for the Fe1 and Fe2 centers.[12,21] When increasing the temperature to 300 K, the Fe2–N bond lengths significantly increase to 2.071(5)–2.259(5) Å, in good agreement with those of reported HS Fe^{II} compounds with an N_6 coordination environment. While the Fe1–C and Fe1–N bond lengths are nearly unchanged (1.917(4)–1.937(6) Å, 2.001(5)–2.016(4) Å, respectively), suggesting the LS Fe^{III} for the Fe1 center. The Fe2–N bond lengths are 1.887(17)–2.033(14) Å at 100 K and 2.079(9)–2.221(10) Å at 300 K for **2**, 1.938(2)–2.009

Table 1 Crystallographic data for compounds **1**, **2**, and **3**

	1		**2**		**3**	
Formula	$C_{70}H_{88}B_2Fe_4N_{26}O_{10}P_2S_2$		$C_{74}H_{78}B_2Cl_4Fe_4N_{28}O_3P_2Se_2$		$C_{76}H_{96}B_4Fe_4N_{28}O_6P_2$	
M_r/g mol^{-1}	1824.69		2014.28		1826.33	
T, K	100	300	100	300	100	300
Crystal system	Orthorhombic	Orthorhombic	Orthorhombic	Orthorhombic	Orthorhombic	Orthorhombic
Space group	*Fdd*2	*Fdd*2	*Fdd*2	*Fdd*2	*Fdd*2	*Fdd*2
a, Å	28.476(3)	29.674(5)	28.952(13)	29.79(3)	28.913(5)	29.677(18)
b, Å	47.057(4)	47.644(9)	47.23(2)	47.45(6)	47.393(8)	47.38(3)
c, Å	13.3974(14)	13.108(3)	13.137(7)	13.324(17)	13.020(2)	13.027(9)
β, °	90	90	90	90	90	90
V, Å^3	17 953(3)	18 532(6)	17 965(15)	18 832(40)	17 841(5)	18 318(19)
Z	8	8	8	8	8	8
D_{cal}/g cm^{-3}	1.223	1.210	1.490	1.232	1.203	1.172
2θ range/°	4.492–55.1	5.23–50.084	5.308–50.446	4.39–49.752	5.328–50.292	4.4–41.872
Completeness	98.8%	98.0%	98.1%	98.7%	98.9%	98.6%
Residual map, e Å^{-3}	0.34/−0.50	0.42/−0.28	1.10/−0.84	0.29/−0.34	0.31/−0.20	0.33/−0.29
GOF on F^2	1.010	1.057	1.016	0.912	1.020	1.026
Final indices [$I > 2\sigma(I)$]	R_1 = 0.0280	R_1 = 0.0397	R_1 = 0.0855	R_1 = 0.0592	R_1 = 0.0257	R_1 = 0.0520
	wR_2 = 0.0687	wR_2 = 0.1112	wR_2 = 0.2100	wR_2 = 0.1254	wR_2 = 0.0629	wR_2 = 0.1198

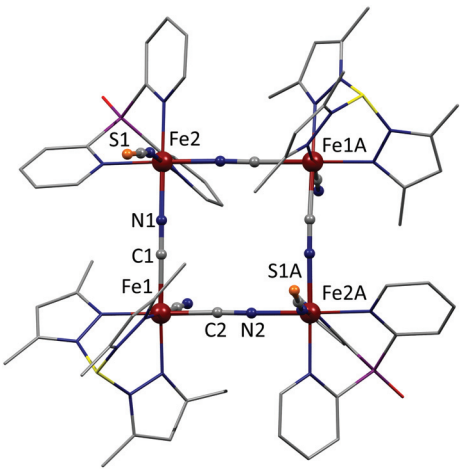

Fig. 1 The molecular structure of **1** at 100 K. The hydrogen atoms and lattice solvents are omitted for clarity [symmetry transformation: A = *–x, –y, –z*].

(2) Å at 100 K and 2.030(8)–2.130(6) Å at 300 K for **3** (Table 2). The shorter bond variations in the Fe2 site indicate the partial LS–HS transition of **2** and **3** at 300 K. Both Fe1–N and Fe1–C bond distances for **2** and **3** showed similar variations with **1** (Tables S1 and S2†).

To further evaluate the spin state change at the Fe2 site of **1** to **3**, the distortion indices Σ (the sum of the deviations from 90° of the 12 *cis*-angles of the FeN_6 octahedron) and Θ (the sum of the deviation from 60° of the 24 trigonal angles of the projection of the [FeN_6] octahedron onto its trigonal faces)[22] were calculated and are listed in Table 2. Generally, an entropy-favoured HS Fe^{II} ion adopts a more distorted octahedral geometry with much larger distortion parameters than those for its LS state. As a result, the Σ and Θ values at 100 K showed a significant increase with varying degrees in comparison with those at 300 K, (Σ/Θ = 13.33/34.67, (100 K) → 34.05/66.23 (300 K) for **1**; Σ/Θ = 12.93/41.71, (100 K) → 31.94/62.82 (300 K) for **2**; Σ/Θ = 11.35/32.56, (100 K) → 21.30/47.42 (300 K) for **3**). All these observations above are in accordance with the magnetic properties (vide post).

Variable-temperature (VT) IR spectra were measured to track the spin transition process. Overall, for compounds **1**, **2**, and **3**, the absorption peak located at 2151 cm^{-1} and the shoulder near 2138 cm^{-1} are ascribed to the characteristic cyanide vibrations of the {Fe^{III}–CN–Fe^{II}} species and the terminal cyanide groups of the [(Tp*)$Fe^{III}(CN)_3$]$^-$ units.[10a,c,23] Only small shifts have been observed for them in the VT-IR spectra, which further suggests that the oxidation state in the Fe1 site remains unchanged. However, the absorption peaks for the co-ligand (ν_{NCE}) are clearly dependent on the spin state change of the Fe2 center. At 310 K, **1** exhibited an absorption peak at 2063 cm^{-1} which is assigned to the cyanide group stretching of the NCS^- (ν_{NCS}) group.[9,24] As the temperature was lowered to 150 K, the ν_{NCS} stretching peak for the HS phase decreased in intensity and a new peak appeared at 2109 cm^{-1} (Fig. 2). Similar spectral changes were also observed for compounds **2** and **3**, where the ν_{NCSe} and ν_{NCBH_3} stretching peaks shifted from 2061 (HS phase) to 2103 cm^{-1} (LS phase) and from 2191 (HS phase) to 2204 cm^{-1} (LS phase), respectively.

Variable-temperature magnetic susceptibility data for the fresh samples of 1–3 were measured under an applied direct current (dc) field of 1 kOe at a sweeping rate of 2 K min^{-1}. The results are shown in Fig. 3 in the form of $\chi_M T$ *versus* T plots (where χ_M is molar magnetic susceptibility and T is temperature). All three compounds showed the complete one-step SCO behaviour. The $\chi_M T$ value of 1.25 cm^3 mol^{-1} K of **1** below 100 K remains nearly constant, in good agreement with the expected value for two LS Fe^{III} (S = 1/2, g = 2.7) and two LS Fe^{II} (S = 0) ions.[10a,12,13] Upon heating, the $\chi_M T$ product underwent a gradual increase centred at 214 K ($T_{1/2}$) and reached a constant value of 8.97 cm^3 mol^{-1} K at above 310 K, typically for two LS Fe^{III} (S = 1/2) and two HS Fe^{II} (S = 2) ions with significant orbital contributions. The continuous $\chi_M T$ *versus* T plots (Fig. S8†) were attributed to the guest-free phase due to the loss of lattice solvents at above 350 K. Specifically, upon cooling and heating, the guest-free sample exhibited a similar and reversible one-step SCO behaviour in a slightly higher temperature range in comparison with that of the solvated phase of **1**. In addition, compounds **2** and **3** exhibited similar SCO behaviours with the $\chi_M T$ values of 8.89 and 1.38 cm^3

Table 2 The selected bond lengths (Å) and distortion parameters of compounds **1**, **2**, and **3**

	1 $^{100\ K}$	**1** $^{300\ K}$	**2** $^{100\ K}$	**2** $^{300\ K}$	**3** $^{100\ K}$	**3** $^{300\ K}$
Fe2–N1	1.947(2)	2.104(4)	1.926(14)	2.088(10)	1.938(2)	2.030(8)
Fe2–N2	1.942(2)	2.117(4)	1.904(13)	2.079(9)	1.948(2)	2.034(7)
Fe2–N4	2.005(2)	2.211(4)	2.004(14)	2.221(10)	1.997(2)	2.130(6)
Fe2–N5	2.001(2)	2.249(4)	1.977(12)	2.183(10)	2.009(2)	2.123(8)
Fe2–N6	2.018(2)	2.259(5)	2.033(14)	2.219(11)	2.008(3)	2.110(10)
Fe2–N7	1.945(3)	2.071(5)	1.887(17)	2.099(14)	1.958(3)	2.034(13)
Fe2–$N_{ave.}$	1.976	2.169	1.955	2.148	1.976	2.077
Σ_{Fe2} [a] [°]	13.33	34.05	12.93	31.94	11.35	21.30
Θ_{Fe2} [b] [°]	34.67	66.23	41.71	62.82	32.56	47.42
$CShM_{Fe2}$ [c]	0.058	0.099	0.70	0.072	0.053	0.055

[a] Σ_{Fe2} is the sum of the deviations from 90° of the 12 *cis* angles of the $Fe2N_6$ octahedron. [b] Θ_{Fe2} is the sum of the deviations from 60° of the 24 trigonal angles of the projection of the [FeN6] octahedron onto its trigonal faces; $CShM_{Fe2}$. [c] is the continuous shape measurement relative to the ideal octahedron of the Fe2 centre.[22b]

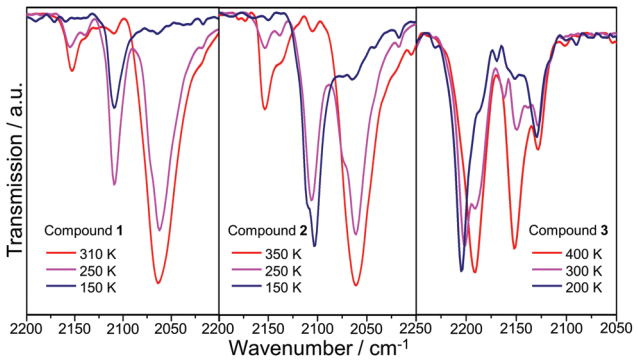

Fig. 2 Variable-temperature IR spectra of compounds **1–3**.

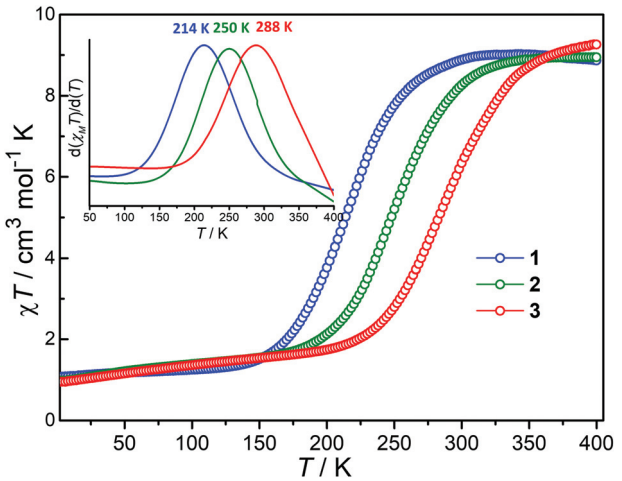

Fig. 3 Variable-temperature susceptibilities of **1**, **2**, and **3** (insert: d($\chi_M T$)/d(T) *versus* T plots used to determine $T_{1/2}$).

mol^{-1} K for the HS and LS state of **2**, respectively, and 9.16 and 1.39 cm^3 mol^{-1} K for **3**, while their transition temperatures shifted to significantly higher temperatures at 250 and 288 K, respectively. It should be mentioned that no obvious thermal hysteresis was observed for all the three compounds (Fig. S8–S10†), indicating the lack of cooperativity due to the weak intermolecular interactions.

To shed light on the SCO behaviours of **1–3**, DFT calculations were applied using the experimental structural data.[25,26] In Table S3,† the computed results indicated that at 100 K both Fe^{II} and Fe^{III} ions in all three compounds are in the LS state (S = 1/2 for Fe^{III,LS}; 0 for Fe^{II,LS}). At 300 K, in **1** and **2**, the Fe^{III} ions remain in the LS state, whereas there is a clear LS → HS (S = 2 for Fe^{II,HS}) transition related to the Fe^{II} ions. For **3**, the Fe^{II} ions are still in the LS state at 300 K. However, the energy difference between the HS and LS states decreases significantly from 12 662 to 1997 cm^{-1} from 100 to 300 K. Therefore, these results confirmed that the increases of the experimental magnetic susceptibilities in **1–3** originate from the LS → HS transitions of the Fe^{II} ions.

To further elucidate the spin transition of the Fe^{II} ions, molecular orbital analysis for **1–3** was performed.[27,28] In **1**, owing to the inversion symmetry of the complex, the evolution of the orbitals of both Fe^{II} ions is symmetry-related to each other; hence, only one of them (the Fe2 site) was considered. The six coordinated atoms around the Fe2 site create a pseudo-octahedral ligand field, which gives rise to the splitting between the 3d orbitals (Fig. 5). Due to the distortion of the perfect symmetry, the degeneracy within each set of orbitals is increased. At 100 K, the energy gap between the t_{2g} and e_g sets (Δ) overcomes the on-site Coulomb interaction between the paired electrons within the orbitals in the t_{2g} set that the LS configuration of the Fe2 center is the most stable state. As shown in Table 2 and S2,† the Fe2–N bonds increase significantly (≈0.2 Å) upon heating, which consequently weakens the ligand-field strength. This leads to the reduction of Δ favoring the HS configuration at 300 K. On the other hand, the LS → HS transition does not occur in the Fe^{III} ions because the Fe^{III}–L bonds are nearly unaffected by the temperature change. In **3**, the increase of Fe^{II}–N bonds at 300 K is not as large as those in **1** and **2** explaining why the spin transition in the former complex is not complete. In addition, the spin density of all complexes is plotted in Fig. 4, which also strongly supports the orbital analysis. The magnetic exchange interaction between the Fe^{III} ions was also studied by the broken-symmetry approach (Table S4†). The obtained results demonstrated that

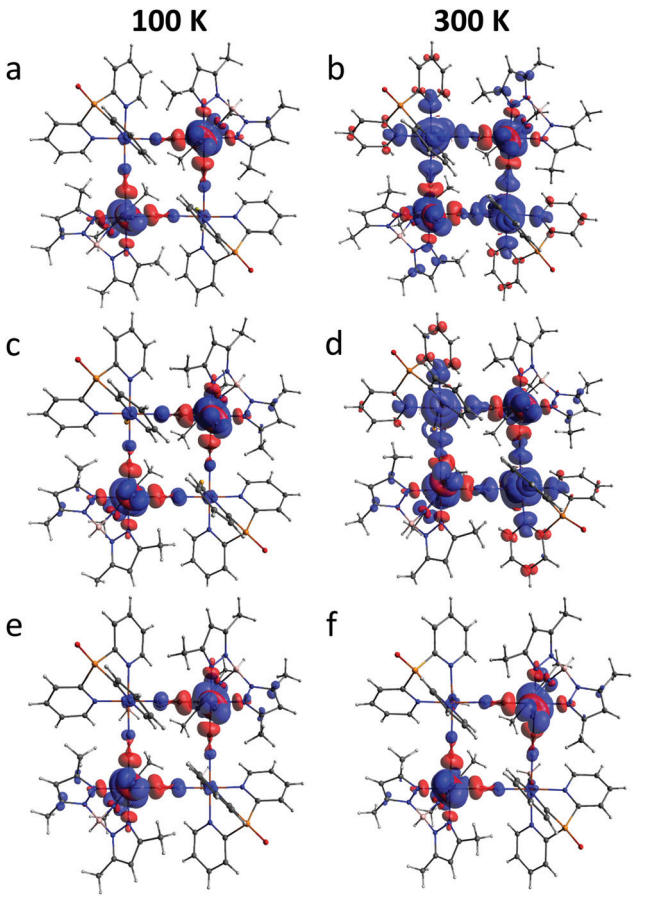

Fig. 4 Spin density plots of (a) **1** at 100 K, (b) **1** at 300 K, (c) **2** at 100 K, (d) **2** at 300 K, (e) **3** at 100 K, and (f) **3** at 300 K.

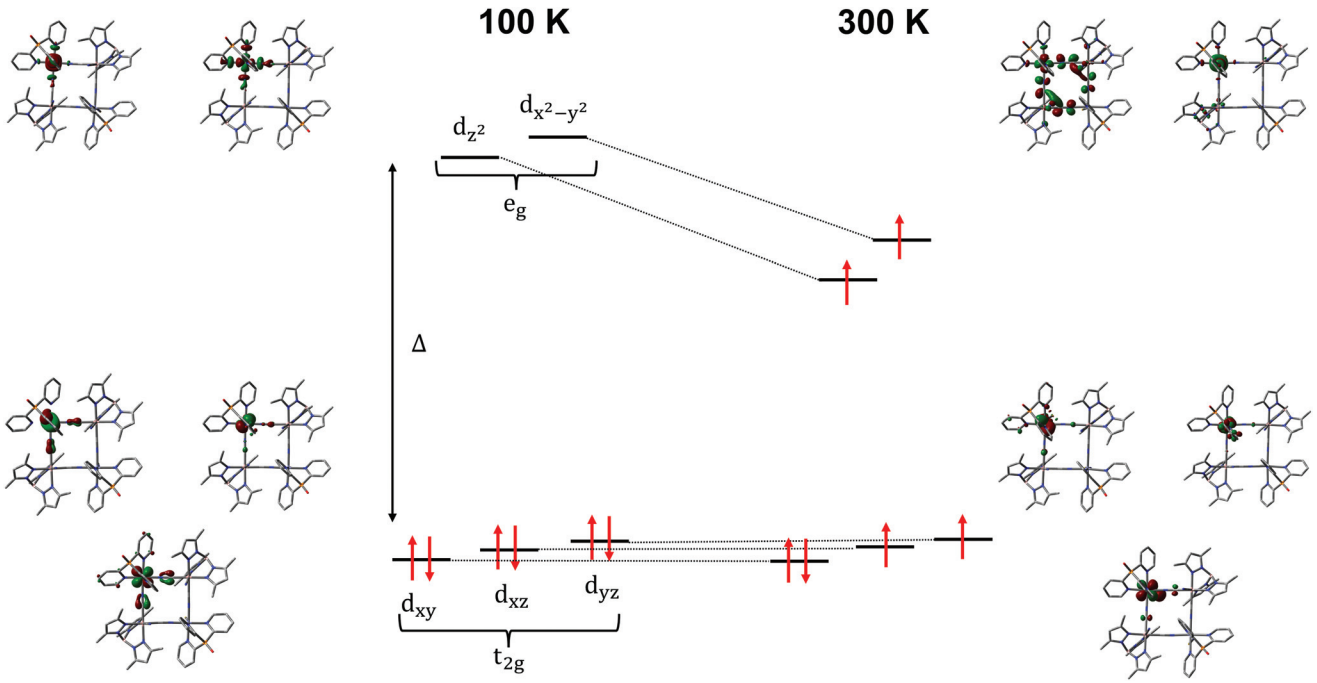

Fig. 5 Schematic molecular orbital diagram for Fe^{2+} in **1** at 100 K and 300 K.

the exchange strength is about a few wavenumbers and plays a negligible role in the magnetic properties within the investigated temperature range. In conclusion, the DFT calculations are in good agreement with the experiments on the thermal SCO phenomenon observed in all complexes.

Conclusions

In conclusion, a new synthetic strategy by incorporating both tridentate capping ligands of TPPO and monodentate NCE^- co-ligands around the Fe(II) centres was successfully employed to prepare three neutral $\{Fe_2^{III}Fe_2^{II}\}$ molecular squares in the well-studied $[(Tp^R)Fe(CN)_3]^-$ family. Detailed magnetic, structural and DFT calculation studies demonstrated that all the three compounds exhibit thermally induced reversible SCO with a tuneable transition temperature ($T_{1/2}$). The shift of $T_{1/2}$ from 214 to 250 to 288 K for **1**, **2**, and **3** is due to the increasing ligand field from NCS^- to $NCSe^-$ to $NCBH_3^-$.[29] The synthetic strategy developed in this work can be used to explore other tridentate capping ligands, which should allow for rational tuning of the ligand field strength as well as the redox potential to achieve multi-stable materials. Studies in this direction are currently underway in our lab.

Experimental section

Materials and physical measurements

All of the starting materials were commercially available and used without further purification. $[(PPh_3Me)][(Tp^*)Fe^{III}(CN)_3]$ and TPPO were prepared according to literature methods.[30]

Variable-temperature infrared (IR) spectra were obtained over the range of 4000–600 cm^{-1} on a Bruker Tensor II spectrophotometer equipped with a low temperature golden gate controller by using liquid nitrogen. Elemental analysis (EA) for C, H, O and N was performed on an Elementar Vario EL Cube elemental analyzer. Power X-ray diffraction (PXRD) patterns were recorded on a Rigaku Smartlab X-ray diffractometer. Thermogravimetric analysis (TGA) was carried out under an argon atmosphere at 3 K min^{-1} using a METTLER-TOLEDO TG2 instrument. Magnetic measurements were performed on a Quantum Design SQUID MPMS3 magnetometer on the microcrystals of fresh samples **1–3**. Diamagnetic corrections were calculated from Pascal constants and applied to all constituent atoms and the sample holder.[31]

Caution! Although no problems were encountered during this work, cyanide is highly toxic. Thus, these starting materials should be handled in small quantities and with great caution.

Synthesis of $\{[(Tp^*)Fe^{III}(CN)_3]_2[Fe^{II}(TPPO)]_2[NCS]_2\}\cdot 2CH_3OH\cdot 6H_2O$ (1)

A solution of tridentate ligand TPPO (0.025 mmol, 7.03 mg) in 3 mL of dichloromethane was added dropwise to a well-stirred solution of $Fe(OTf)_2$ (0.025 mmol, 8.85 mg) and $[(PPh_3Me)][(Tp^*)Fe^{III}(CN)_3]$ (0.025 mmol, 17.75 mg) in acetonitrile (2 mL). The dark red solution that formed was stirred for 20 minutes before adding to a solution of KSCN (0.025 mmol, 2.43 mg) in 3 mL of methanol. The resulting mixture was stirred for another 5 minutes and then filtered. Dark red block single crystals were obtained by slow evaporation of the filtrate at room temperature after one week. Yield:

18 mg, 43.6%. Elem anal. (%) Calcd (found) for $C_{68}H_{68}B_2Fe_4N_{26}O_2P_2S_2$: C, 49.42 (49.35); H, 4.15 (4.11); N, 22.04 (21.98). IR (KBr, 300 K): ν_{CN} 2152, 2138 cm^{-1}; ν_{NCS} 2063, 2109 cm^{-1}; ν_{BH} 2540 cm^{-1}.

Synthesis of $\{[(Tp^*)Fe^{III}(CN)_3]_2[Fe^{II}(TPPO)]_2[NCSe]_2\}\cdot 2MeCN\cdot 2CH_2Cl_2\cdot 2H_2O$ (2)

Complex **2** was obtained with a similar procedure to that of **1**, except replacing the KSCN ligand with the KSeCN ligand. Yield: 20 mg, 45.3%. Elem anal. (%) Calcd (found) for $C_{68}H_{68}B_2Fe_4N_{26}O_2P_2Se_2$: C, 46.77 (46.72); H, 3.92 (3.89); N, 20.85 (20.82). IR (KBr, 300 K): ν_{CN} 2153, 2136 cm^{-1}; ν_{NCSe} 2061, 2103 cm^{-1}; ν_{BH} 2539 cm^{-1}.

Synthesis of $\{[(Tp^*)Fe^{III}(CN)_3]_2[Fe^{II}(TPPO)]_2[NCBH_3]_2\}\cdot 4CH_3OH\cdot 2MeCN$ (3)

Complex **3** was obtained with a similar procedure to that of **1**, except replacing the KSCN ligand with the $NaNCBH_3$ ligand. Yield: 16 mg, 39.7%. Elem anal. (%) Calcd (found) for $C_{68}H_{68}B_4Fe_4N_{26}O_2P_2$: C, 50.73 (50.69); H, 4.25 (4.21); N, 22.62 (22.55). IR (KBr, 300 K): ν_{CN} 2162, 2150, 2129 cm^{-1}; ν_{NCBH_3} 2204, 2191 cm^{-1}; ν_{BH} 2543 cm^{-1}.

Computational details

Density functional theory (DFT) calculations

The investigation of the spin multiplicity of individual Fe sites in the $\{Fe_2^{III}Fe_2^{II}\}$ compounds was performed with the ORCA 5.0 package[32,33] using the experimental X-Ray structures. The other Fe^{2+} and Fe^{3+} ions were replaced with their diamagnetic Zn^{2+} and Ga^{3+} analogues, respectively. The following parameters were chosen:

- DFT functional: B3LYP[34]
- Basis set: DKH-def2-TZVP[35,36]
- Convergence strategy: NORMALSCF
- Charge of compound: 0
- Spin multiplicity: 2, 4, and 6 for Fe^{III} ions; 1, 3, and 5 for Fe^{II} ions.

Conflicts of interest

There are no conflicts to declare.

Acknowledgements

This work was supported by the Stable Support Plan Program of the Shenzhen Natural Science Fund (no. 20200925151834005), the National Natural Science Foundation of China (no. 21901108, 22173043), and the start-up fund from SUSTech. L. U. acknowledges the financial support of the research projects R-143-000-A65-133 and R-143-000-A80-114 of the National University of Singapore. *Ab initio* calculations were done on the ASPIRE-1 cluster (http://www.nscc.sg) under the project 11001278.

Notes and references

1 P. Gütlich and H. A. Goodwin, *Spin Crossover in Transition Metal Compounds I, II, and III*, Springer-Verlag, Berlin, Germany, 2004.
2 M. A. Halcrow, *Spin-crossover materials: properties and applications*, John Wiley & Sons, 2013.
3 A. B. Gaspar, V. Ksenofontov, M. Seredyuk and P. Gütlich, *Coord. Chem. Rev.*, 2005, **249**, 2661–2676.
4 Y.-S. Meng and T. Liu, *Acc. Chem. Res.*, 2019, **52**, 1369–1379.
5 (*a*) K. S. Murray, H. Oshio and J. A. Real, Eds. Special Issue on Spin-Crossover Complexes, *Eur. J. Inorg. Chem.*, 2013, **5–6**, 574–1067; (*b*) O. Kahn and C. J. Martinez, *Science*, 1998, **279**, 44–48; (*c*) P. Gütlich, Y. Garcia and T. Woike, *Coord. Chem. Rev.*, 2001, **219**, 839–879; (*d*) P. Gütlich, A. Hauser and H. Spiering, *Angew. Chem., Int. Ed. Engl.*, 1994, **33**, 2024–2054; (*e*) O. Sato, J. Tao and Y.-Z. Zhang, *Angew. Chem., Int. Ed.*, 2007, **46**, 2152–2187.
6 (*a*) S. Decurtins, P. Gütlich, C. P. Köhler and H. Spiering, *Chem. Phys. Lett.*, 1984, **105**, 1–4; (*b*) K.-P. Xie, Z.-Y. Ruan, B.-H. Lyu, X.-X. Chen, X.-W. Zhang, G.-Z. Huang, Y.-C. Chen, Z.-P. Ni and M.-L. Tong, *Angew. Chem., Int. Ed.*, 2021, **60**, 27144–27150; (*c*) B. Brachňaková and I. Šalitroš, *Chem. Pap.*, 2018, **72**, 773–798.
7 (*a*) S. Brooker, *Chem. Soc. Rev.*, 2015, **44**, 2880–2892; (*b*) M. A. Halcrow, *Chem. Soc. Rev.*, 2011, **40**, 4119–4142; (*c*) I. Šalitroš, N. T. Madhu, R. Boča, J. Pavlik and M. Ruben, *Monatsh. Chem.*, 2009, **140**, 695–733; (*d*) J. Krober, E. Codjovi, O. Kahn, F. Groliere and C. Jay, *J. Am. Chem. Soc.*, 1993, **115**, 9810–9811.
8 (*a*) J. Tao, R. J. Wei, R. B. Huang and L. S. Zheng, *Chem. Soc. Rev.*, 2012, **41**, 703–737; (*b*) Y.-F. Deng, Y.-N. Wang, X.-H. Zhao and Y.-Z. Zhang, *CCS Chem.*, 2021, **3**, 3277–3288; (*c*) I. Šalitroš, O. Fuhr, A. Eichhöfer, R. Kruk, J. Pavlik, L. Dlháň, R. Boča and M. Ruben, *Dalton Trans.*, 2012, **41**, 5163–5171; (*d*) I. Šalistroš, O. Fuhr and M. Ruben, *Materials*, 2016, **9**, 585–594; (*e*) J.-Y. Ge, Z. Chen, L. Zhang, X. Liang, J. Su, M. Kurmoo and J.-L. Zuo, *Angew. Chem., Int. Ed.*, 2019, **58**, 8789–8793; (*f*) H.-Y. Wang, J.-Y. Ge, C. Hua, C.-Q. Jiao, Y. Wu, C. F. Leong, D. M. D'Alessandro, T. Liu and J.-L. Zuo, *Angew. Chem., Int. Ed.*, 2017, **56**, 5465–5470.
9 H. Hagiwara and S. Okada, *Chem. Commun.*, 2016, **52**, 815–818.
10 (*a*) Y.-Z. Zhang, F.-D. Li, R. Clérac, M. Kalisz, C. Mathonière and S. M. Holmes, *Angew. Chem., Int. Ed.*, 2010, **49**, 3752–3756; (*b*) Y.-Z. Zhang, P. Ferko, D. Siretanu, R. Ababei, N. P. Rath, M. J. Shaw, R. Clérac, C. Mathonière and S. M. Holmes, *J. Am. Chem. Soc.*, 2014, **136**, 16854–156864; (*c*) S.-H. Liu, Y.-F. Deng, Z.-Y. Chen, L.-Y. Meng, X.-Y. Chang, Z.-P. Zheng and Y.-Z. Zhang, *CCS Chem.*, 2020, **2**, 2530–2538; (*d*) J. Yang, Y.-F. Deng, X.-Y. Zhang, X.-Y. Chang, Z.-P. Zheng and Y.-Z. Zhang, *Inorg. Chem.*, 2019, **58**, 7127–7130; (*e*) Y. Cheng, Z.-Y. Chen, K.-P. Xie, Y.-F. Deng, Y.-X. Jiang, Q. Liu and Y.-Z. Zhang, *Inorg. Chem.*, 2020, **59**, 8025–8033; (*f*) L.-Y. Meng, Y.-F. Deng, S.-H. Liu,

Z.-P. Zheng and Y.-Z. Zhang, *Sci. China: Chem.*, 2021, **64**, 1340–1348.
11 S. Kang, H. Zheng, T. Liu, K. Hamachi, S. Kanegawa, K. Sugimoto, Y. Shiota, S. Hayami, M. Mito, T. Nakamura, M. Nakano, M. L. Baker, H. Nojiri, K. Yoshizawa, C.-Y. Duan and O. Sato, *Nat. Commun.*, 2015, **6**, 1–6.
12 J.-X. Hu, Y.-S. Meng, L. Zhao, H.-L. Zhu, L. Liu, Q. Liu, C.-Q. Jiao and T. Liu, *Chem. – Eur. J.*, 2017, **23**, 15930–15936.
13 A. Mondal, Y. Li, P. Herson, M. Seuleiman, M. L. Boillot, E. Riviere, M. Julve, L. Rechignat, A. Bousseksou and R. Lescouëzec, *Chem. Commun.*, 2012, **48**, 5653–5655.
14 J. Glatz, L.-M. Chamoreau, A. Flambard, J.-F. Meunier, A. Bousseksou and R. Lescouëzec, *Chem. Commun.*, 2020, **56**, 10950–10953.
15 T. Liu, H. Zheng, S. Kang, Y. Shiota, S. Hayami, M. Mito, O. Sato, K. Yoshizawa, S. Kanegawa and Y.-C. Duan, *Nat. Commun.*, 2013, **4**, 1–7.
16 H. Zheng, Y. S. Meng, G. L. Zhou, C. Y. Duan, O. Sato, S. Hayami, Y. Luo and T. Liu, *Angew. Chem., Int. Ed.*, 2018, **57**, 8468–8472.
17 (*a*) J.-T. Chen, X.-H. Zhao and Y.-Z. Zhang, *Dalton Trans.*, 2020, **49**, 5949–5956; (*b*) X.-H. Zhao, D. Shao, J.-T. Chen, M. Liu, T. Li, J. Yang and Y.-Z. Zhang, *Dalton Trans.*, 2021, **50**, 9768–9774; (*c*) X.-H. Zhao, D. Shao, J.-T. Chen, D.-X. Gan, J. Yang and Y.-Z. Zhang, *Sci. China: Chem.*, 2022, **65**, 532–538.
18 M. You, D.-X. Gan, Y.-F. Deng, D. Shao, Y.-S. Meng, X.-Y. Chang and Y.-Z. Zhang, *CCS Chem.*, 2021, **3**, 2593–2600.
19 (*a*) B. Fei, X.-Q. Chen, Y.-D. Cai, J.-K. Fang, M.-L. Tong, J. Tucek and X. Bao, *Inorg. Chem. Front.*, 2018, **5**, 1671–1676; (*b*) Y.-S. Ye, X.-Q. Chen, Y.-D. Cai, B. Fei, P. Dechambenoit, M. Rouzières, C. Mathonière, R. Clérac and X. Bao, *Angew. Chem., Int. Ed.*, 2019, **58**, 18888–18891.
20 (*a*) W. Wen, Y.-S. Meng, C.-Q. Jiao, Q. Liu, H.-L. Zhu, Y.-M. Li, H. Oshio and T. Liu, *Angew. Chem., Int. Ed.*, 2020, **59**, 16393–16397; (*b*) K. Zhang, S. Kang, Z.-S. Yao, K. Nakamura, T. Yamamoto, Y. Einaga, N. Azuma, Y. Miyazaki, M. Nakano, S. Kanegawa and O. Sato, *Angew. Chem., Int. Ed.*, 2016, **55**, 6047–6050; (*c*) M. Nihei, M. Ui, M. Yokota, L. Han, A. Maeda, H. Kishida, H. Okamoto and H. Oshio, *Angew. Chem., Int. Ed.*, 2005, **44**, 6484–6487; (*d*) W. Huang, X. Ma, O. Sato and D. Wu, *Chem. Soc. Rev.*, 2021, **50**, 6832–6870.
21 (*a*) C. Zheng, J. Xu, F. Wang, J. Tao and D. Li, *Dalton Trans.*, 2016, **45**, 17254–17263; (*b*) C. Zheng, S. Jia, Y. Dong, J. Xu, H. Sui, F. Wang and D. Li, *Inorg. Chem.*, 2019, **58**, 14316–14324; (*c*) A. Sulaiman, Y.-Z. Jiang, M.-K. Javed, S. Q. Wu, Z.-Y. Li and X.-H. Bu, *Inorg. Chem. Front.*, 2022, **9**, 241–248.
22 (*a*) R. Ketkaew, Y. Tantirungrotechai, P. Harding, G. Chastanet, P. Guionneau, M. Marchivie and D. J. Harding, *Dalton Trans.*, 2021, **50**, 1086–1096; (*b*) J. Cirera, E. Ruiz and S. Alvarez, *Organometallics*, 2005, **24**, 1556–1562.
23 M. Nihei, Y. Sekine, N. Suganami, K. Nakazawa, A. Nakao, H. Nakao, Y. Murakami and H. Oshio, *J. Am. Chem. Soc.*, 2011, **133**, 3592–3600.
24 (*a*) A. Arroyave, A. Lennartson, A. Dragulescu-Andrasi, K. S. Pedersen, S. Piligkos, S. A. Stoian, S. M. Greer, C. Pak, O. Hietsoi, H. Phan, S. Hill, C. J. McKenzie and M. Shatruk, *Inorg. Chem.*, 2016, **55**, 5904–5913; (*b*) D. Zhu, Y. Xu, Z. Yu, Z. Guo, H. Sang, T. Liu and X. You, *Chem. Mater.*, 2002, **14**, 838–843; (*c*) X.-Y. Chen, R.-B. Huang, L.-S. Zheng and J. Tao, *Inorg. Chem.*, 2014, **53**, 5246–5252.
25 J. Cirera and E. Ruiz, *Comments Inorg. Chem.*, 2019, **39**, 216–241.
26 S.-G. Wu, M. N. Hoque, J.-Y. Zheng, G.-Z. Huang, N. V. Ha Anh, L. Ungur, W.-X. Zhang, Z.-P. Ni and M.-L. Tong, *CCS Chem.*, 2021, **3**, 453–459.
27 J. Cirera and F. Paesani, *Inorg. Chem.*, 2012, **51**, 8194–8201.
28 J. Cirera and E. Ruiz, *Inorg. Chem.*, 2018, **57**, 702–709.
29 X.-Q. Chen, Y.-D. Cai, J.-K. Fang, Y.-S. Ye, M.-L. Tong and X. Bao, *Inorg. Chem. Front.*, 2019, **6**, 2194–2199.
30 (*a*) D. Li, S. Parkin, G. Wang, G.-T. Yee and S. M. Holmes, *Inorg. Chem.*, 2006, **45**, 1951–1959; (*b*) T. Gneuß, M.-J. Leitl, L.-H. Finger, N. Rau, H. Yersin and J. Sundermeyer, *Dalton Trans.*, 2015, **44**, 8506–8520.
31 R. L. Carlin, *Magnetochemistry*, Springer-Verlag Press, Berlin, Heidelberg, 1986.
32 F. Neese, *Wiley Interdiscip. Rev.: Comput. Mol. Sci.*, 2012, **2**, 73–78.
33 F. Neese, *Wiley Interdiscip. Rev.: Comput. Mol. Sci.*, 2018, **8**, e1327.
34 P. J. Stephens, F. J. Devlin, C. F. Chabalowski and M. J. Frisch, *J. Phys. Chem.*, 1994, **98**, 11623–11627.
35 D. A. Pantazis and F. Neese, *J. Chem. Theory Comput.*, 2009, **5**, 2229–2238.
36 D. Aravena, F. Neese and D. A. Pantazis, *J. Chem. Theory Comput.*, 2016, **12**, 1148–1156.